Hindawi
Geofluids
Volume 2022, Article ID 7016581, 11 pages
https://doi.org/10.1155/2022/7016581

Research Article

Experimental Study on Damage and Degradation of Structure Plane in Rock Mass under Cyclic Shear Load

Rubao Hong[1,2] **Wenbin Jian**[1,3] **Deng Zhang**[1] **and Ruimin Chen**[1,3]

[1]*Institute of Geotechnical and Geological Engineering, Fuzhou University, Fuzhou 350108, China*
[2]*Fujian Center of Geo-Environmental Monitoring, Fuzhou 350001, China*
[3]*Key Laboratory of Geohazard Prevention of Hilly Mountains, Ministry of Land and Resources, Fuzhou 350003, China*

Correspondence should be addressed to Wenbin Jian; jwb@fzu.edu.cn

Received 8 April 2022; Accepted 19 May 2022; Published 11 June 2022

Academic Editor: Yu Wang

By summarizing the generalized model of the structural plane in a rock mass under a cyclic shear load and influencing factors of dynamic mechanical properties of the structural plane, the mechanism of structural plane damage and degradation is discussed, and the evolution of damage to the structural plane is ascertained from cyclic shear tests by using structural planes with different undulating angles. Based on model tests and previous studies, nonlinear constitutive equations considering the effect of structural plane damage and degradation are presented. The effects of the initial undulating angle, amplitude of the cyclic shear load, and cycle times on the strength of the structural plane, as well as the degeneration process of structural plane stiffness under a cyclic shear load, are taken into consideration in the equations. The applicability of the above-mentioned constitutive equations is analyzed with a corresponding program compiled in the FISH language in the Universal Distinct Element Code (UDEC). The UDEC numerical simulation results are verified with ones from the model test. The achievements presented in this paper are of great significance to theoretical study of the mechanical behaviors of rock masses under cyclic shear loads and to project practice.

1. Introduction

A series of macroscopic and microscopic geologic defects can form in rock masses during lengthy geological ages [1–3]. The rock slope and the static and dynamic responses of structural planes are all decisive factors [4, 5]. Therefore, study of the static and dynamic responses of structural planes is essential groundwork for investigating rock slope fatigue, which is of great theoretical and practical significance. Structural plane statics is of extensive concern, and great achievements have been achieved, but thorough study of the dynamic characteristics of structural planes is still inadequate because of the restrictions of theoretical and experimental conditions. Because rock samples with natural structural surfaces are difficult to obtain and their physical and mechanics parameters vary widely, reliable laws are not easy to ascertain by conducting tests.

Some research on the dynamic characteristics of structural planes of rock masses has been done. Jafari et al. [6] proposed a conceptual model of the strain–stress relation of structural planes in rock masses under a cyclic shear load by using mortar to simulate the structural plane. Lee et al. [7] put forward a joint damage coefficient and an equivalent undulation angle and proposed an elastoplastic constitutive model in which the degradation of second-order asperities was taken into consideration by laboratory cyclic shear tests. Homand et al. [8] calculated joint surface roughness and defined joint surface degradation, developing two new peak strength criteria related to joint surface degradation. Research on the effect of undulating angles, normal stress, and the strength of the rock wall on structural planes of rock masses has been conducted by Liu et al. [9]. After reviewing tests and numerical models of rock interfaces and joints under cyclic shear loading, Yin et al. [10] developed a new constitutive model, in which the dilation relation causing coupling of the normal and shear responses was considered. Peng et al. [11] proposed an improved hierarchical model of rock joints based on Plesha's constitutive model, which can

simulate the mechanism of elastic deformation, sliding, damage, shear-off, crush, and separation of joints. Yan et al. [12] used finite difference method to study the dynamic response law of rock slope with structural plane. Zhou et al. [13] and Song et al. [14] summarized the displacement response law and stress wave propagation law of different parts of weak surface under blasting load. Zhao et al. [15] combined theoretical analysis with the sandstone sliding friction test to propose a model to predict the friction coefficient of sandstone joint. The results showed that the larger the wear mass, the larger the friction coefficient in sliding, and the larger the wear area, the smaller the friction coefficient.

Kamonphet et al. [16] performed direct shear tests to determine the peak and residual shear strengths of fractures in sandstone, granite, and limestone under cyclic shear loading. Results indicate that the cyclic shear load can significantly reduce the fracture shear strengths and stiffness. Liu et al. [17] conducted prepeak cyclic shear tests and mesonumerical simulations to investigate the macro-mesocumulative damage mechanism of the weak layer considering the impacts of various factors and to investigate the regularities of the shear strength, shear deformation, and other mechanical properties of joint rock mass with different roughnesses under compression-shear stress by Zhou et al. [18]. Marble specimens were prepared with the dentate height of 0, 1, and 3 mm, respectively. Then, direct shear tests were conducted on the marble specimens under different normal stresses. Experiment results show that the climbing-gnawing process of joints goes through four stages: the compaction stage, the climbing stage, the saw-tooth cutting stage, and the completely crushing stage. Wang et al. [19–21] studied the characteristics of rock mass instability under different conditions from the influence of freeze–thaw on rock microstructure change and fatigue mechanical behaviors, rock instability induced by cyclic uniaxial increasing-amplitude decreasing-frequency (CUIADF) loads, and the structural deterioration and associated macro-mesofracture behaviors of granite containing crack-like and hole-like flaws subjected to multilevel cyclic loads. Xing et al. [22] used cement mortar of different strengths to duplicate the artificial split joints with different morphologic parameters and tested 48 split rock joints replicas by direct shear apparatus under constant normal stress to obtain the shear strength and stress ratio (shear strength/normal stress) of rock joints under different test conditions. And a modified model was proposed on the foundation of BARTON's shear strength criterion by introducing material strength correction term. Liu et al. [23] conducted cyclic shear tests on 3D rough joint surfaces under constant normal stiffness boundary conditions to reveal the effects of the normal stiffness and the number of cyclic shearing on the shear stress, normal deformation, normal stress, shear stress path, surface resistance index, acoustic emission responses, and surface wear characteristics of joint surfaces.

In this article, the mechanisms of damage and degradation of structural planes are discussed by conducting cyclic shear tests with structural planes of different undulating angles. Based on model tests, nonlinear constitutive equa-

Table 1: Similitude laws and constants of the model.

Physical quantity	Similarity law	Affinity constant
Material density (ρ)	C_ρ	1.5
Cohesive strength (C)	$C_c = C_\rho C_L$	15
Internal friction angle (ϕ)	$C_\phi = 1$	1
Poisson's ratio (μ)	$C_u = 1$	1
Uniaxial compressive strength (σ)	$C_\sigma = C_\rho C_L$	15
Modulus of elasticity (E)	$C_E = C_\rho C_L$	15

Table 2: Main physical and mechanical parameters of the simulation materials according to similarity theory.

Physical quantity	ρ (g/cm^3)	σ (MPa)	E (GPa)	μ	C (MPa)	ϕ (°)
Actual rock	2.6	42.3	23.25	0.19	9.3	40
Test sample	1.76	2.83	1.55	0.19	0.62	40

Figure 1: Homemade cyclic shear apparatus for rock mass testing.

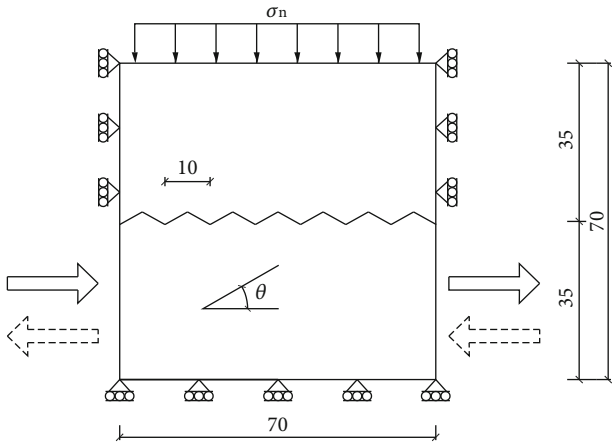

Figure 2: Sample loading process (units = mm).

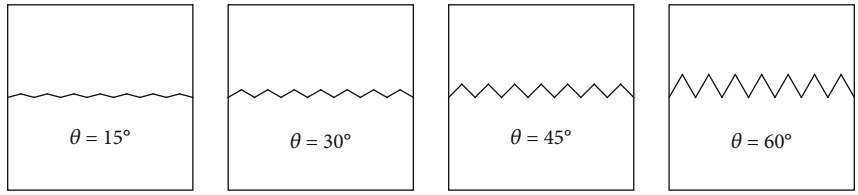

Figure 3: Samples with different undulating angles.

Table 3: Groups and numbers of samples.

Group	Undulating angle (°)	No. of samples	Serial number
1	15	5	A-15-1~A-15-5
2	30	5	B-30-1~B-30-5
3	45	5	C-45-1~C-45-5
4	60	5	D-60-1~D-60-5

tions considering the effect of damage and degradation of structural planes are also presented. The effects of initial undulating angle, amplitude of the cyclic shear load, and cycle times on the strength of the structural plane, as well as the degeneration of structural plane stiffness under cyclic shear loading, are furthermore taken into consideration in the equations. The applicability of the above-mentioned constitutive equations is analyzed with a corresponding program compiled in the FISH language in the Universal Distinct Element Code (UDEC). The numerical simulation results from UDEC are verified with ones from the model test.

2. Cyclic Shear Test of the Structural Plane

2.1. Material and Test Equipment. To overcome the difficulty in obtaining rock samples with natural structural planes in cyclic shear tests, we use similarity theory to conduct model tests using similar materials to ensure consistency of samples. Sandstone is widely distributed in Fujian Province and has the characteristics of a large number of joints and fissures, which often causes geological disasters of rock landslide. The sandstone samples, which are moderately weathered rocks, are from the construction site at the Sanming Shaxian Airport. The test samples are made up of sand, cement, and gypsum in the proportions of 3 : 0.4 : 0.6. The similitude law and similitude constant of the model are given in Table 1. The main physical and mechanical parameters of actual rock samples and simulation materials according to the similarity theory are given in Table 2.

The loading device for testing was remodeled from a rock direct shear testing instrument, as shown in Figure 1. The remodeled instrument has made special optimization for cyclic shear conditions, in which multiple mechanical tests can be carried out on the interview samples of rock mass structure, including structural plane monotonic shear test and structural plane cyclic shear test. The sample loading process is shown in Figure 2. The upper half of the sample was fixed, and a vertical load of 0.5 MPa was applied, and the lower half was pushed by the loading device to shear the sample. Both stress and displacement of the sample were measured in the shearing process.

2.2. Experimental Process. To reveal the effect of the structural plane on the shear strength of rock, samples with different undulating angles of 15°, 30°, 45°, and 60° were made, as shown in Figure 3. The length of the boss was 1 cm, the size of the mold was $70.7 \times 70.7 \times 70.7$ mm, and the size of the test sample was $70 \times 70 \times 70$ mm.

Four groups of experiments were conducted. The groupings and serial numbers are listed in Table 3. Samples were sheared ten times in each group. Samples were retreated to their initial position after shearing for the next loop.

2.3. Experimental Results. The characteristic stress–strain curves of the first five cycles is shown in Figure 4. From Figure 4, we can see that the peak shear stress decreases rapidly as the number of cycles increases. The shapes of the stress–strain curves remain almost unchanged after 2 to 4 cycles of shear while the peak stresses decrease slightly. Shearing stiffness tends to decrease gradually as the number of cycles increases, which means that the stiffness of the structural plane degenerates with the increase of cycle times.

The shear strength ratio R_f, a nondimensional parameter, is used herein to measure the deterioration of shear strength with cycle times and defined as

$$R_f = \frac{\tau_i}{\tau_0}, \tag{1}$$

where τ_0 is the peak shear stress in the first cycle and τ_i is the peak shear stress in the cycle i.

The relationship between the shear strength ratio and circulation time is shown in Figure 5. As can be seen from Figure 5, the shear strength ratio of the sample remains almost unchanged after five cycles of shear. The shear strength ratios of structural planes with different undulating angles vary from each other. The greater the undulating angle, the more serious the deterioration of shear strength of the structural plane becomes in the first five cycles.

Figure 6 shows how the convergent values of the shear strength ratio change with different undulating angles. The convergent values of the shear strength ratio $R(t)$ decay with different undulating angles in a negative exponential form as follows:

$$R(t) = Q_0 + (1 - Q_0)e^{-c\theta}, \tag{2}$$

where Q_0 and c are undetermined coefficients and θ is the undulating angle of the structural plane.

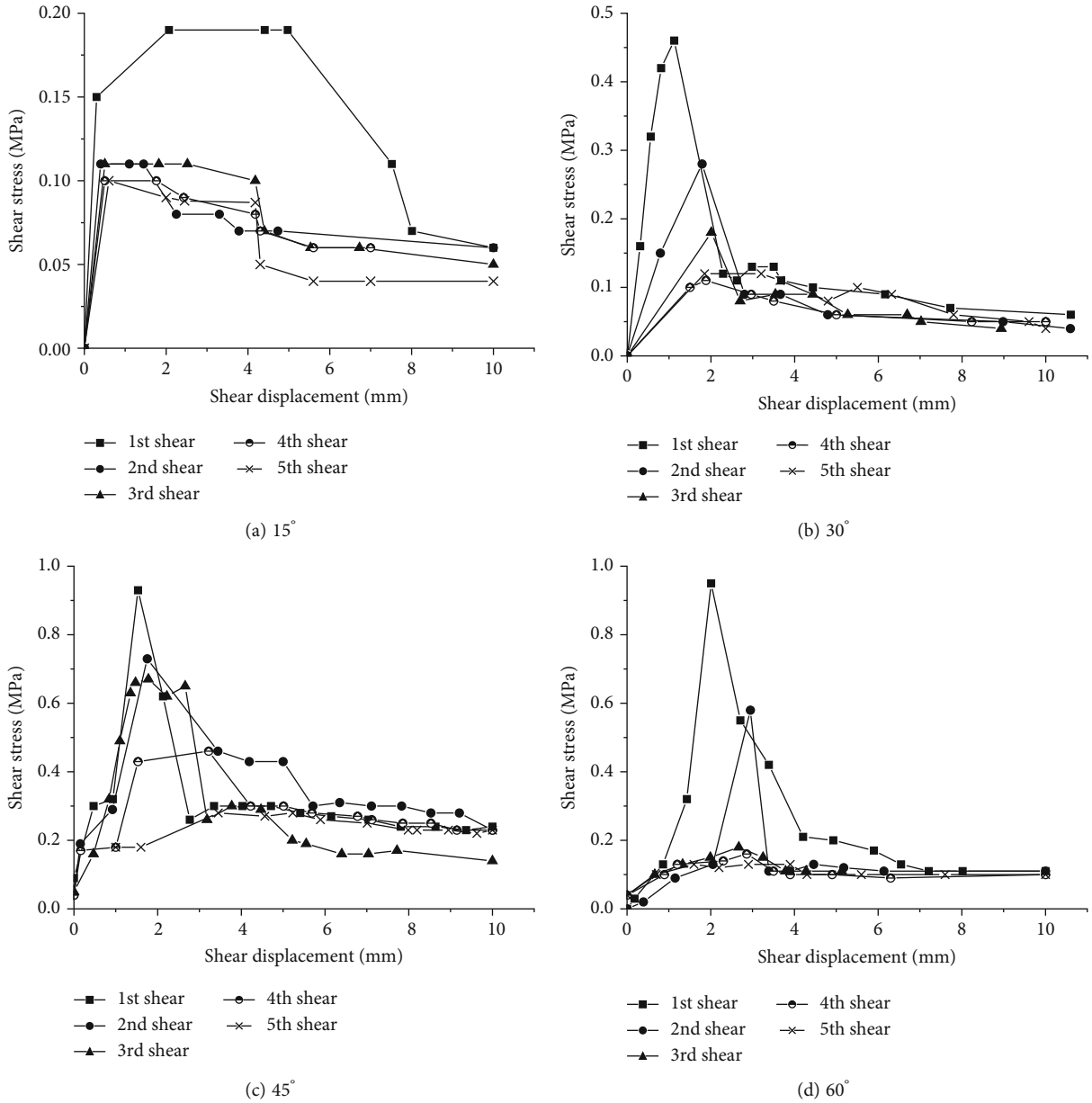

Figure 4: Displacement–stress curve of structural planes with different undulating angles under cyclic shear loading.

A fitting curve can be obtained after a regression fitting of the experimental results in Figure 6. The correlation coefficient of fitting is 0.97221, which means that the fitting curve is in good correlation with experiment results. The fitting result shows that $Q_0 = 0.03867$ and $c = 0.05619$; that is, the undulating angle has great influence on the shear strength ratio. The minimum of the shear strength ratio may reach to 0.03867, which is lower than the shear strength derived from the internal friction angle of the rock. The reason of this difference may be that the structural plane is filled by shearing substances and sliding friction is substituted for rolling friction during the shearing process.

2.4. Deterioration Mechanism of the Structural Plane under a Cyclic Shear Load. It is not difficult to speculate that deterioration of the structural plane under a cyclic shear load occurs because bosses of the structural plane are extruded and evened off; that is, there is a decrease of roughness and undulation of the structural plane. Roughness refers to large-scale and macroundulations of the structural plane, while undulation refers to partial and rough extent of the structural plane (see Figure 7).

Study of shear wear of structural planes has been most challenging; thus, digital images and scanning electron microscope are used to conduct the research. To observe the change of the roughness of the structural plane under a cyclic shear load, a test sample was taken out after shearing was done at each time, and the structural plane was scanned to get the digital images of structural plane. An electron microscope was used to observe the change of undulation of the structural plane, which is tiny and difficult to observe by the naked eye in general.

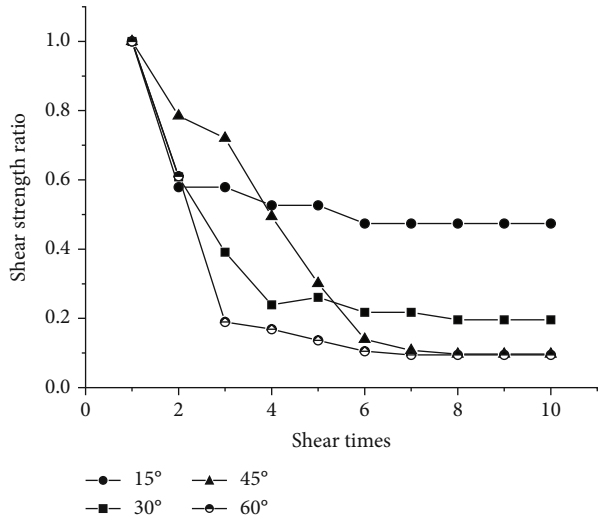

Figure 5: Relationship between shear strength ratio and shear times.

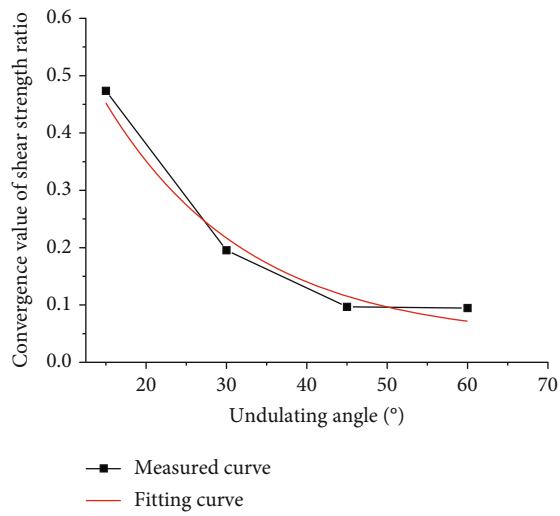

Figure 6: Curves of convergence value of shear strength ratio.

Structural planes with an undulating angle of 60° under a cyclic shear load are of great discreteness, and sometimes, the damage occurs in the rock mass but not in the structural plane. Hence, the mechanism of injury to the structural planes with undulating angles of 15°, 30°, and 45° was therefore considered. The wear conditions of structural planes with an undulating angle of 45° under a cyclic shear load are shown in Figure 8, which shows clearly that the deterioration of the structural plane under a cyclic shear load occurs because bosses of the structural plane are evened off.

For the structural plane with an undulating angle of 15°, most pointed ends of the bosses were pared away, and the structural plane was flattened. Clast filling in the structural plane increases inconspicuously with the increase of cycle times.

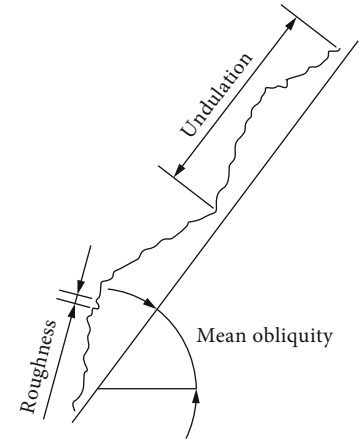

Figure 7: Roughness and undulation of structural planes.

For the structural plane with an undulating angle of 30°, the pointed ends of the bosses were seriously damaged but their shapes were not fundamentally destroyed under the first shear. Boss shapes were obviously damaged, and the structural plane was filled by mast clast under the second shear. The amount of clast increases significantly after the third shear.

The situation for the structural plane with an undulating angle of 45° was similar to that with an undulating angle of 30°. The bosses of structural plane were completely destroyed after the third shear.

The bosses of structural planes with different undulating angles under a cyclic shear load were extruded and evened off gradually, and a powdery substance engendered by the boss damage entered into the gap between structural planes. With the increase of undulating angle, the amount of powdery substance also increased gradually. The increase of powdery substance results in the change of the structural plane from sliding friction to rolling friction in the shearing process. This is also the reason why the convergence value of the shear strength ratio decreases with the increase of undulating angle. That is, the larger the undulating angle is, the more amounts of the powdery substance enter into structural plane, and the structural plane changes more easily from sliding friction to rolling friction. Because the mechanical properties of both sides of the structural plane with different undulating angles are similar, the final convergence values of the shear strength are approximate. As the initial shear strength of the structural plane with a large undulating angle is greater, the shear strength ratio is reduced more.

The roughness of the structural plane with an undulating angle of 45° during cyclic shearing was observed by electron microscope at a magnification of 85x (see Figure 9). As can be seen, the particles are interbedded on the surface, and the surface is undulating and irregular before shearing. As the number of cycles increases, the protruding parts of the surface are smoothed gradually, and the extent of grinding increases. This indicates that the roughness of the structural plane decreases with cyclic shear and that the surface is progressively flattened. This is also an important reason for deterioration of the structural plane.

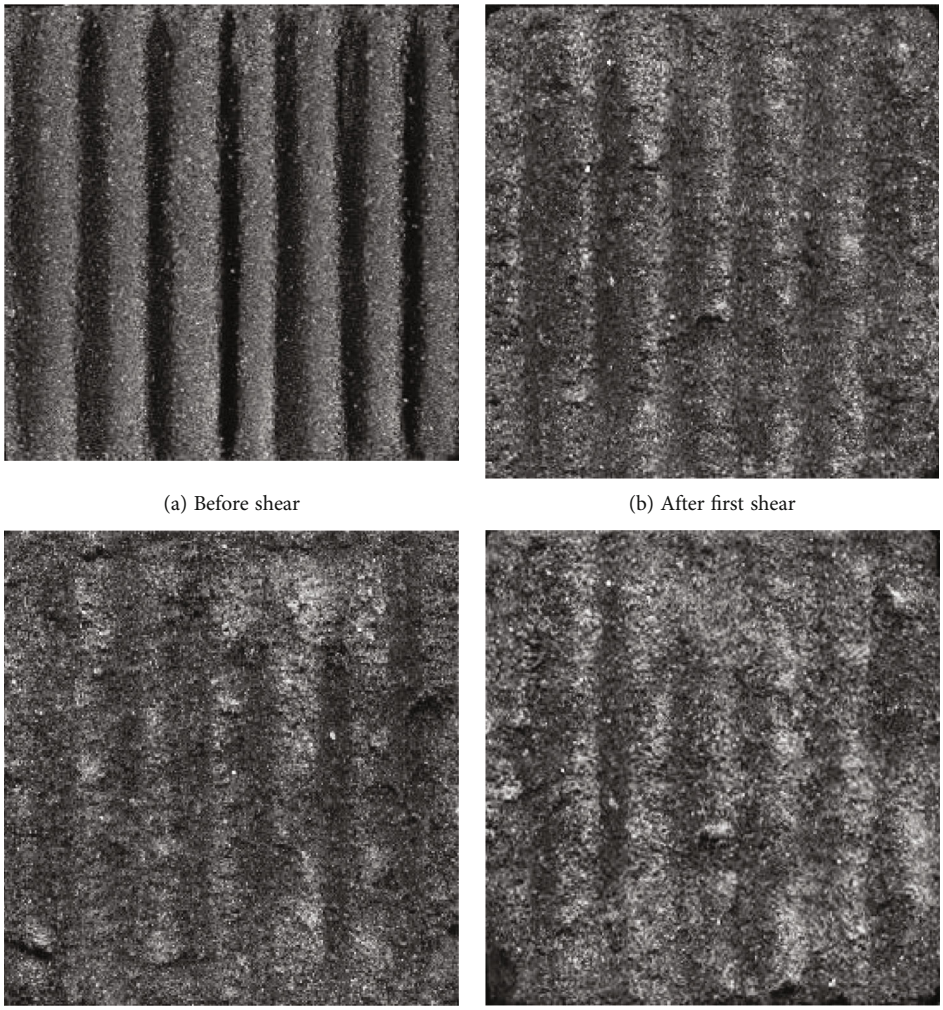

(a) Before shear (b) After first shear

(c) After second shear (d) After third shear

Figure 8: Wear conditions of structural planes with an undulating angle of 45° under a cyclic shear load.

3. Constitutive Relation for the Structural Plane under a Cyclic Shear

The constitutive relation for the structural plane under a cyclic shear is now inferred based on analysis of the experimental data and research results. An elastic–perfectly plastic constitutive model is employed, and a modified Mohr–Coulomb criterion formula considering the cyclic shear is taken as the yield function. The derivation is as follows.

An incremental constitutive equation is adopted, and relative displacement is assumed to consist of elastic deformation and plastic deformation. The following coordinate system is set up as shown in Figure 10.

$$\{d\varepsilon\} = \{d\varepsilon^e\} + \{d\varepsilon^p\}, \tag{3}$$

For the elastic part, the stress tensor can be expressed as follows:

$$\{d\sigma\} = [D]\{d\varepsilon^e\}, \tag{4}$$

where the stiffness matrix $[D]$ can be represented as

$$[D] = \begin{bmatrix} k_{nn} & k_{ns} \\ 0 & k_{ss}(t) \end{bmatrix}. \tag{5}$$

Because only the tangential displacement is considered to affect the normal displacement, we get $k_{sn} = 0$. Because the degradation of tangential stiffness of the structural plane is the main factor affecting slope stability, only degradation of tangential stiffness is considered while the normal stiffness and dilatancy rigidity are assumed to remain unchanged.

For the plastic part, the plastic strain increment can be expressed as the following equation according to Ref. [24]:

$$\{d\varepsilon^p\} = \begin{cases} 0, & F(\sigma, H) < 0, \\ \lambda\left\{\dfrac{\partial G}{\partial \sigma}\right\}, & F(\sigma, H) = 0, \end{cases} \tag{6}$$

where F is the yield function, H is the hardening function, G is the potential function, and λ is a nonnegative constant.

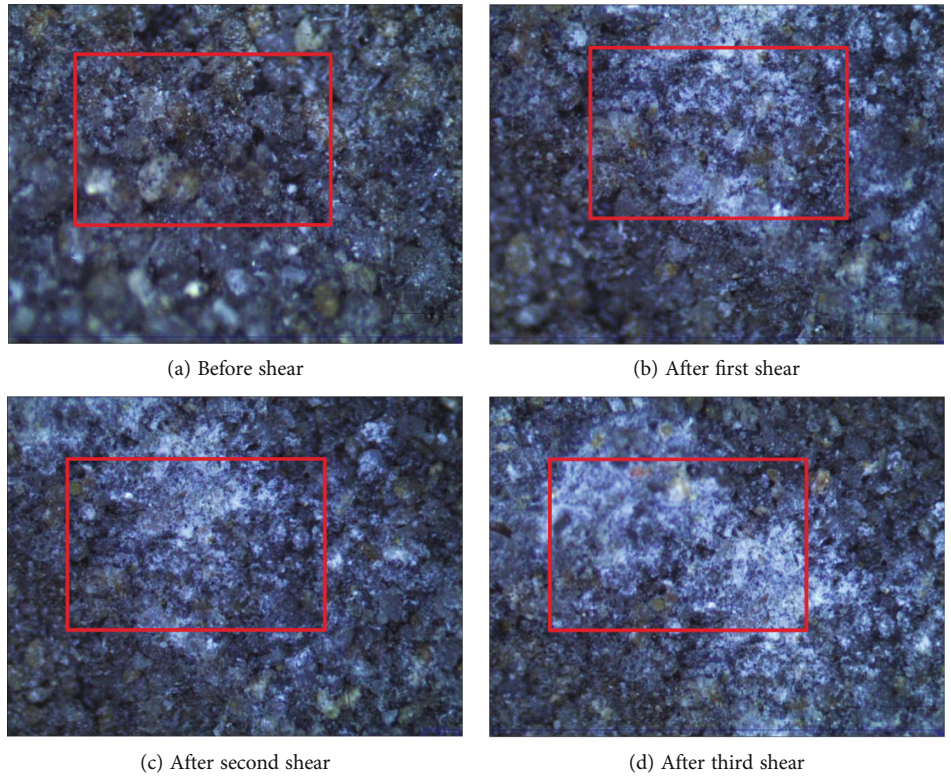

(a) Before shear (b) After first shear

(c) After second shear (d) After third shear

Figure 9: Change of roughness of structural planes.

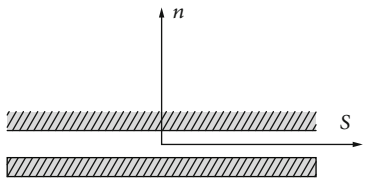

Figure 10: Coordinate system of the structural plane.

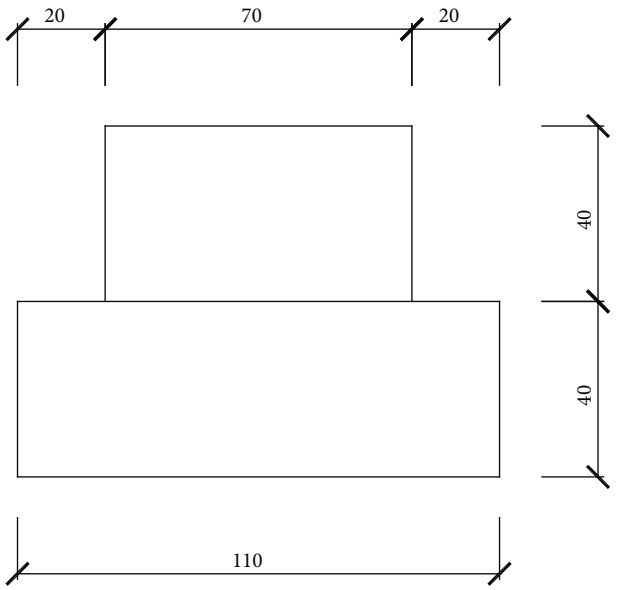

Figure 11: Generalized model of the structural plane under a cyclic shear load (units = mm).

If the plastic work is taken as the hardening function, the total differential of the yield function becomes zero. That is,

$$\left\{\frac{\partial F}{\partial \sigma}\right\}^T \{d\sigma\} + \frac{\partial F}{\partial W^P} dW^P = 0, \tag{7}$$

$$dW^P = \{\sigma\}^T \{d\varepsilon^P\}, \tag{8}$$

From Equations (3), (4), and (6), the following formula is obtained:

$$\{d\sigma\} = [D]\left(\{d\varepsilon\} - \lambda\left\{\frac{\partial G}{\partial \sigma}\right\}\right). \tag{9}$$

Substituting Equations (6) and (9) into Equation (7) then gives

$$\left\{\frac{\partial F}{\partial \sigma}\right\}^T [D]\left(\{d\varepsilon\} - \lambda\left\{\frac{\partial G}{\partial \sigma}\right\} + \lambda \frac{\partial F}{\partial W^P}\{\sigma\}^T \left\{\frac{\partial G}{\partial \sigma}\right\}\right) = 0. \tag{10}$$

The nonnegative constant λ can be solved for by using Equations (6) in Equation (10) or

$$\lambda = \frac{\{\partial F/\partial \sigma\}^T [D]}{\{\partial F/\partial \sigma\}^T [D]\{\partial G/\partial \sigma\} - \partial F/\partial W^P \{\sigma\}^T \{\partial G/\partial \sigma\}} \{d\varepsilon\}. \tag{11}$$

Table 4: Physical and mechanical parameters of the rock mass.

Material density ρ(g/cm^3)	Bulk modulus K (MPa)	Shear modulus G (MPa)
2.6	4.3×10^4	2.6×10^4

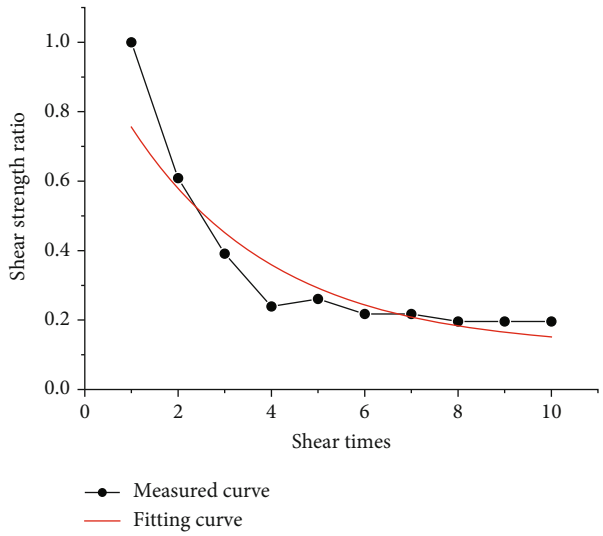

Figure 12: Fitting curves of structural plane parameters with an undulating angle of 30°.

Table 5: Physical and mechanical parameters of the structural plane.

Normal stiffness K_n (MPa)	Shear stiffness K_s (MPa)	Internal friction angle φ (°)	Q_0	$R(t)$	a	b	c
2×10^4	545	42.6	0.039	0.117	0.324	0.150	0.056

Substituting Equation (11) into Equation (9) gives the elastoplastic stress–strain relationship of the structural plane:

$$\{d\sigma\} = \left(\frac{[D]\{\partial G/\partial\sigma\}\{\partial F/\partial\sigma\}^T[D]}{\{\partial F/\partial\sigma\}^T[D]\{\partial G/\partial\sigma\} - \partial F/\partial W^P\{\sigma\}^T\{\partial G/\partial\sigma\}} \right)\{d\varepsilon\}. \tag{12}$$

Here, the modified Mohr–Coulomb criterion formula considering the deterioration of the structural plane cyclic shear is taken as the yield function, so

$$F = |\sigma_1| + \sigma_2 D(t) \tan\varphi - D(t)C, \tag{13}$$

$$G = |\sigma_1|, \tag{14}$$

where $D(t)$ is defined as the deterioration factor of the structural plane, which is used to characterize the dynamic attenuation of the shear strength of the structural plane with cyclic shear times.

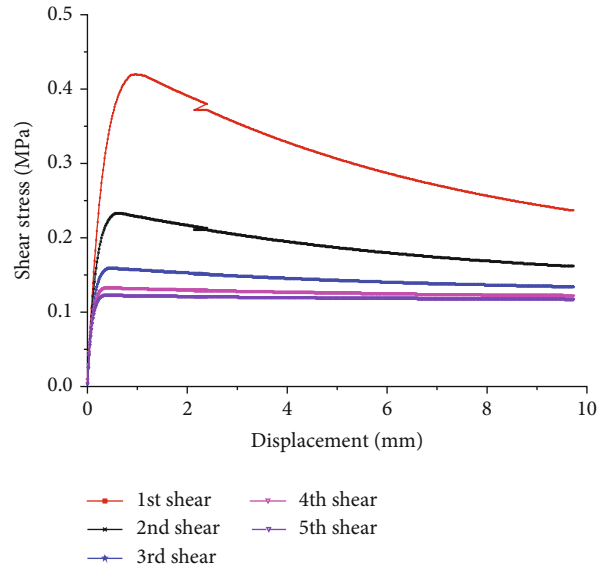

Figure 13: Discrete element simulation results.

The constitutive relation for the structural plane under a cyclic shear can be solved to get expressions for $D(t)$ in Equation (12) and $k_{ss}(t)$ in Equation (5).

The deterioration factor of the structural plane $D(t)$ and degradation factor of the tangential stiffness of the structural plane $k_{ss}(t)$ can be obtained by the following formulas.

(1) $D(t)$

Ni et al. [25] considered that vibration wear and relative speed have a relatively independent impact on the structural plane, and the equation for the coefficient of vibration deterioration can be expressed as follows:

$$D(t) = \gamma(t)\eta(t), \tag{15}$$

where $\gamma(t)$ is the influence coefficient of relative speed while $\eta(t)$ is the influence coefficient of vibration wear.

$\eta(t)$ is determined by the following equation according to test data:

$$\eta(t) = \delta(t) + (1 - \delta(t))e^{-\mathrm{an}}, \tag{16}$$

where $\delta(t)$ is the convergence of influence coefficient of vibration wear, a is a coefficient to be confirmed, and n is cyclic shear times.

$\delta(t)$ is related to the amplitude of cyclic shear as

$$\delta(t) = R(t) + (1 - R(t))e^{-bJ(t)}, \tag{17}$$

where $R(t)$ is the convergence value and $J(t)$ is the amplitude of cyclic shear.

The initial fluctuation angle has a significant impact on $R(t)$ and can be represented as

$$R(t) = Q_0 + (1 - Q_0)e^{-c\theta}. \tag{18}$$

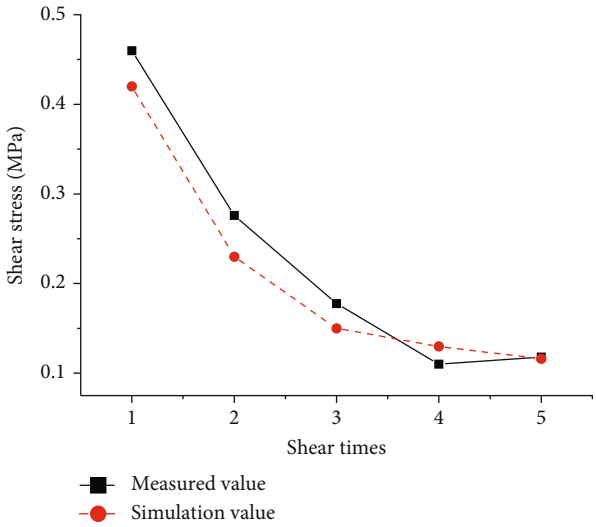

Figure 14: Experimental and simulated results for the peak value of shear stress.

The influence of the shear rate on the mechanical properties of the structural plane is not yet fully accounted for. Wang et al. [26] deem that the dynamic friction factor of the structural plane changes randomly with the shear rate, while Wang and Zhang [27] consider the dynamic friction factor of structural plane to be an even function whose value decreases when the absolute value of relative velocity increases progressively. Therefore, the influence of the shear rate on the dynamic friction factor is not taken into consideration, which means that degradation of the structural plane is only in relation to vibration wear. Therefore, $\gamma(t) = 1$. Accordingly, the expression for $D(t)$ can be obtained by substituting Equations (16)–(18) into Equation (15).

(2) $k_{ss}(t)$

According to Ref. [26], the expression for degradation of the tangential stiffness of the structural plane is

$$k_{ss}(t) = k_{ss0}\left(1 - \frac{R\tau(t)}{\tau_m(t)}\right), \tag{19}$$

where R is a constant close to 1 and usually taken as 0.98 in general, k_{ss0} is the initial tangential stiffness, $\tau(t)$ is the tangential stress, and $\tau_m(t)$ is the shear strength of the structural plane and determined by Equation (13). Based on the above deduction, the constitutive relation for the structural plane under a cyclic shear is obtained by substituting the expressions for $D(t)$ and $k_{ss}(t)$ into Equation (12).

4. Discrete Element Analysis of the Structural Plane under a Cyclic Shear

4.1. Calculation Model. A generalized model was built to perform a numerical simulation of structural plane properties under a cyclic shear load. The research problem was simplified as a plane stress problem. The size of the model was 70 × 70 mm with, the central section cut by a perforated structural plane (see Figure 11). During the numerical test, the displacement of the lower rock block was restricted, and a normal force was imposed on upper rock block to simulate the impact of the normal force on the structural plane. A reciprocating motion of the upper rock block was imposed to simulate cyclic shear.

The main steps of establishing the model are as follows.

4.1.1. Programming the Constitutive Relation of the Structural Plane under a Cyclic Shear. The Mohr–Coulomb criterion considering the deterioration of structural plane under cyclic shear was taken as the yield function, and the elastic–perfectly plastic constitutive model was then employed. The constitutive relation for structural plane under a cyclic shear was programmed using the FISH language and applied in the UDEC program successfully.

4.1.2. Acquisition and Analysis of the Stress and Displacement of the Structural Plane. Constitutive models within the discrete element method use nodes of the structural plane; the stress and displacement of which are inhomogeneous. The stress and displacement measured from a direct shear test of rock are actually average values. To ensure the numerical simulation results comparable to actual test results, it is essential to calculate the average stress and displacement. A self-compiled FISH code was used in the computing process. The basic working process was as follows:

(1) Apply a normal load

(2) Evaluate the initial value by summing the stress and displacement of each node of the structural plane

(3) Apply a tangential displacement

(4) Evaluate the summation of the stress and displacement of each node at the structural plane once again

(5) Count the summation of the nodes for the structural plane

(6) Sum the values of stress and displacement minus the initial ones and divide by the sum of nodes to get the average value

4.1.3. Physical and Mechanical Parameters of the Rock Mass and Structural Plane. The rock mass was simplified as an elastic model, and the physical and mechanical parameters are listed in Table 4.

Results of the structural plane test with an undulating angle of 30° were used to assign the model parameters. Parameters Q_0 and c were obtained from the fitting in Figure 6. Parameters $R(t)$ and a were obtained from Figure 12 (fitted using Equation (16)). Accordingly, the physical and mechanical parameters of the structural plane were assigned (see Table 5).

4.2. Validation of the Constitutive Model. The simulation results are shown in Figure 13. It can be seen that although an ideal elastoplastic model was adopted, the cyclic shear constitutive model taken in this study still reflects the post

Table 6: Constructive models of the structural plane in the rock mass under a cyclic shear load.

Model	Sticking–sliding characteristics	Wear characteristics	Nonlinear dilatancy	Stiffness degeneration	Number of parameters
This study	Positive	Positive	Negative	Positive	8
Ref. [10]	Positive	Positive	Positive	Positive	12
Ref. [25]	Positive	Positive	Negative	Negative	6

peak characteristics of the structural plane to some extent by considering the deterioration of strength parameters in the yield criterion. Yet, the simulation result at postpeak is approximate.

A comparison between experimental and simulation results is shown in Figure 14. According to the figure, the structural plane strength obtained from the discrete element method is close to that from the experiments. With the increase in cycle times, the difference between the experimental and simulation results gets smaller and smaller and, basically, the same after five cycles. The maximum difference at the peak shear stresses is 8%, which relatively meets the engineering requirements.

4.3. Comparison of Various Constitutive Models. Comparison results of the constitutive model used in this study and those of Refs. [10, 25] are given in Table 6. The factors affecting the structural plane are more considered in this study, and characteristics of the structural plane for the constitutive model in Ref. [10] are much close to those of the real structural plane. However, the number of parameters of the constitutive model in Ref. [10] is up to 12. The constitutive model in Ref. [25] has fewer parameters, but it is poorly applicable for the deformation problem as it cannot reflect the stiffness degradation characteristics of the structural plane.

The nonlinear dilatancy of the structural plane is neglected in this study, which may introduce some errors into the calculation. As the stability of the structural plane is mainly controlled by tangential displacement, main controlling factors of the structural plane are taken into consideration, and appropriate simplifications are made in this study. Therefore, parameter acquisition is relatively simple, and the constitutive model has greater applicability. However, it should be made clear that the model is not applicable when the nonlinear dilatancy characteristics of structural plane need to be considered.

5. Conclusion

(1) Under a cyclic shear load, the deterioration of macroscopic mechanical properties of the structural plane arises, as verified by the reduction in the strength parameters of the structural plane and degradation of the stiffness of the structural surfaces. Strength reduction of the structural plane is related to the amplitude of cyclic shear, times of cyclic shear, and undulating angles of the structural plane. The intensity parameters generally decline exponentially with the increase of these three factors, and a convergent value exists. The convergent shear strength ratio $R(t)$ decay with different undulating angles in a negative exponential form, or $R(t) = Q_0 + (1 - Q_0)e^{-c\theta}$

(2) Particles are interbedded on the surface. These surfaces are undulating and irregular before shearing. As the number of cycles increases, protruding parts of the surface are gradually smoothened, and the extension of the grinding increases. This indicates that the roughness of the structural plane decreases with cyclic shear and the surface may be progressively flattened. This is also the primary reason for deterioration of the structural plane

(3) Based on the main controlling factors of dynamic instability of the rock slope, the strength deterioration and stiffness degradation properties of the structural plane under cyclic shear conditions are considered in the constitutive model of the structural plane derived in this study. The parameter acquisition of the proposed constitutive model is relatively simple and verified by experimental results. This model may be more applicable

(4) The formulas and conclusions obtained from the test are mainly based on the moderately weathered sandstone taken from the study area, and their applicability needs to be further verified by subsequent relevant tests

Data Availability

Data available are available from the corresponding author upon request.

Conflicts of Interest

The authors declare that they have no conflicts of interest.

Acknowledgments

This work was financially supported by the National Natural Science Foundation of China (grant no. 41072232) and Natural Science Foundation of Fujian Province (grant no. 2010J01254).

References

[1] C. B. Yan, *Study on Cumulative Damage Effects and Stability of Rock Mass under Blasting Loading*, Central South University, 2006.

[2] X. H. Ni, X. J. Li, and Z. D. Zhu, "Quantitative test study of meso-damage of granite under cyclic load with different

frequencies," *Rock and Soil Mechanics*, vol. 33, no. 2, pp. 422–427, 2012.

[3] X. H. Ni, Z. D. Zhu, J. Zhao, D. W. Li, and X. T. Feng, "Meso-damage mechanical digitalization test of complete process of rock failure," *Rock and Soil Mechanics*, vol. 30, no. 11, pp. 3283–3290, 2009.

[4] S. J. Wang and S. Y. Xue, "Dynamic analysis of wedge sliding on rock slopes," *Chinese Journal of Geology*, vol. 4, no. 2, pp. 177–182, 1992.

[5] C. Y. Wang and S. J. Wang, "Study on stability of the bank slope of Ertan reservoir under seismic condition," *Rock Mass Engineering Geological Mechanics Problems*, vol. 7, 1987.

[6] M. K. Jafari, K. A. Hosseini, F. Pellet, M. Boulon, and O. Buzzi, "Evaluation of shear strength of rock joints subjected to cyclic loading," *Soil Dynamic and Earthquake Engineering*, vol. 23, no. 7, pp. 619–630, 2003.

[7] H. S. Lee, Y. J. Park, T. F. Cho, and K. H. You, "Influence of asperity degradation on the mechanical behavior of rough rock joints under cyclic shear loading," *International Journal of Rock Mechanics and Mining Sciences*, vol. 38, no. 7, pp. 967–980, 2001.

[8] F. Homand, T. Belem, and M. Souley, "Friction and degradation of rock joint surfaces under shear loads," *International Journal for Numerical and Analytical Methods in Geomechanics*, vol. 25, no. 10, pp. 973–999, 2001.

[9] B. Liu, H. B. Li, and X. M. Zhu, "Experiment simulation study of strength degradation of rock joints under cyclic shear loading," *Chinese Journal of Rock Mechanics and Engineering*, vol. 30, no. 10, pp. 2033–2039, 2011.

[10] X. J. Yin, G. L. Wang, and C. H. Zhang, "Study of constitutive model for rock interfaces and joints under cyclic shear loading," *Engineering Mechanics*, vol. 22, no. 6, pp. 97–103, 2005.

[11] C. W. Peng, X. R. Zhu, J. C. Wang, and C. Xu, "A hierarchical model of rock joints based on Plesha's constitutive model," *Rock and Soil Mechanics*, vol. 31, no. 7, pp. 2059–2071, 2010.

[12] Z. X. Yan, L. P. Zhang, and X. H. Cao, "Dynamic response and deformation mechanism of a bedding rock slope under earthquakes," *Chinese Journal of Geotechnical Engineering*, vol. 33, no. Supp.1, pp. 54–58, 2011.

[13] J. Zhou, L. Q. Zhang, and R. L. Hu, "Study of rules of stress waves propagation under various attitudes of large-scale fractures," *Chinese Journal of Rock Mechanics and Engineering*, vol. 30, no. 4, pp. 769–780, 2011.

[14] X. L. Song, J. C. Zhang, X. B. Guo, and Z. Xiao, "Influence of blasting on the properties of weak intercalation of a layered rock slope," *International Journal of Mineral, Metallurgy and Materials*, vol. 16, no. 1, pp. 7–11, 2009.

[15] G. C. Zhao, L. G. Wang, N. Zhao, J. Yang, and X. Li, "Analysis of the variation of friction coefficient of sandstone joint in sliding," *Advances in Civil Engineering*, vol. 2020, Article ID 8863960, 12 pages, 2020.

[16] T. Kamonphet, S. Khamrat, and K. Fuenkajorn, "Effects of cyclic shear loads on strength, stiffness and dilation of rock fractures," *Songklanakarin Journal of Science and Technology*, vol. 37, no. 6, pp. 683–690, 2015.

[17] X. R. Liu, B. Xu, X. H. Zhou, Y. K. Xie, C. M. He, and J. H. Huang, "Investigation on macro-meso cumulative damage mechanism of weak layer under pre-peak cyclic shear loading," *Rock and Soil Mechanics*, vol. 42, no. 5, pp. 1291–1303, 2021.

[18] H. Zhou, G. T. Cheng, Y. Zhu, J. Chen, J. J. Lu, and G. J. Cui, "Experimental study of shear deformation characteristics of marble dentate joints," *Rock and Soil Mechanics*, vol. 40, no. 3, pp. 852–860, 2019.

[19] Y. Wang, Z. Y. Song, T. Q. Mao, and C. Zhu, "Macro-meso fracture and instability behaviors of hollow-cylinder granite containing fissures subjected to freeze–thaw–fatigue loads," *Rock Mechanics and Rock Engineering*, vol. 45, pp. 1–21, 2022.

[20] Y. Wang, H. N. Yang, J. Q. Han, and C. Zhu, "Effect of rock bridge length on fracture and damage modelling in granite containing hole and fissures under cyclic uniaxial increasing-amplitude decreasing-frequency (CUIADF) loads," *International Journal of Fatigue*, vol. 158, 2022.

[21] Y. Wang, J. Q. Han, Z. Y. Song, and C. Zhu, "Macro-meso failure behavior of pre-flawed hollow-cylinder granite under multi-level cyclic loads: insights from acoustic emission and post-test CT scanning," *Engineering Fracture Mechanics*, vol. 258, 2021.

[22] W. Z. Xing, S. Wang, and P. X. Fan, "Experimental study on direct shear behavior of split rock joints," *Journal of Central South University(Science and Technology)*, vol. 52, no. 8, pp. 2933–2944, 2021.

[23] R. C. Liu, Q. Yin, H. Q. Yang, H. W. Jing, Y. J. Jiang, and L. Y. Yu, "Cyclic shear mechanical properties of 3D rough joint surfaces under constant normal stiffness(CNS) boundary conditions," *Chinese journal of rock mechanics and Engineering*, vol. 40, no. 6, pp. 1092–1109, 2021.

[24] Y. R. Zheng and L. Kong, *Geotechnical Plasticity*, China Construction Industry Press, 2010.

[25] W. D. Ni, H. M. Tang, and X. Liu, "Dynamic stability analysis of rock slope considering vibration deterioration of structural planes under seismic loading," *Chinese Journal of Rock Mechanics and Engineering*, vol. 32, no. 3, pp. 492–500, 2013.

[26] G. L. Wang, C. H. Zhang, and G. Peng, "Dynamic test of rigid blocks and parameter study in dynamic analysis of distinct elements," *Chinese Journal of Rock Mechanics and Engineering*, vol. 13, no. 2, pp. 124–133, 1994.

[27] S. J. Wang and J. M. Zhang, "On the dynamic stability of block sliding on rock slopes," *Scientia Geologica Sinica*, vol. 2, no. 2, pp. 162–170, 1982.